



Validation of Rapid Magnetic Resonance Myelin Imaging in Multiple Sclerosis

Russell Ouellette, BSc ^{1,2,3,4} Gabriel Mangeat, MSc,^{3,5} Ildiko Polyak, MSc,⁶ Marcel Warntjes, MSc, PhD,^{7,8} Yngve Forslin, MD, PhD,^{1,2} Åsa Bergendal, MSc, PhD,^{1,9} Michael Plattén, MSc, MD,^{1,2,10} Martin Uppman, MSc,^{1,2} Constantina Andrada Treaba, MD, PhD ^{3,4} Julien Cohen-Adad, MSc, PhD,⁵ Fredrik Piehl, MD, PhD,^{1,11} Maria Kristoffersen Wiberg, MD, PhD,^{1,2} Sten Fredrikson, MD, PhD,^{1,11} Caterina Mainero, MD, PhD,^{3,4} and Tobias Granberg, MD, PhD^{1,2,3,4}

Objective: Magnetic resonance imaging (MRI) is essential for multiple sclerosis diagnostics but is conventionally not specific to demyelination. Myelin imaging is often hampered by long scanning times, complex postprocessing, or lack of clinical approval. This study aimed to assess the specificity, robustness, and clinical value of Rapid Estimation of Myelin for Diagnostic Imaging, a new myelin imaging technique based on time-efficient simultaneous T₁/T₂ relaxometry and proton density mapping in multiple sclerosis.

Methods: Rapid myelin imaging was applied using 3T MRI *ex vivo* in 3 multiple sclerosis brain samples and *in vivo* in a prospective cohort of 71 multiple sclerosis patients and 21 age/sex-matched healthy controls, with scan-rescan repeatability in a subcohort. Disability in patients was assessed by the Expanded Disability Status Scale and the Symbol Digit Modalities Test at baseline and 2-year follow-up.

Results: Rapid myelin imaging correlated with myelin-related stains (proteolipid protein immunostaining and Luxol fast blue) and demonstrated good precision. Multiple sclerosis patients had, relative to controls, lower normalized whole-brain and normal-appearing white matter myelin fractions, which correlated with baseline cognitive and physical disability. Longitudinally, these myelin fractions correlated with follow-up physical disability, even with correction for baseline disability.

Interpretation: Rapid Estimation of Myelin for Diagnostic Imaging provides robust myelin quantification that detects diffuse demyelination in normal-appearing tissue in multiple sclerosis, which is associated with both cognitive and clinical disability. Because the technique is fast, with automatic postprocessing and US Food and Drug Administration/CE clinical approval, it can be a clinically feasible biomarker that may be suitable to monitor myelin dynamics and evaluate treatments aiming at remyelination.

ANN NEUROL 2020;87:710–724

View this article online at [wileyonlinelibrary.com](https://www.wileyonlinelibrary.com). DOI: 10.1002/ana.25705

Received May 27, 2019, and in revised form Feb 5, 2020. Accepted for publication Feb 9, 2020.

Address correspondence to Dr Granberg, Department of Neuroradiology, C1-46, Karolinska University Hospital, 141 86, Stockholm, Sweden.

E-mail: tobias.granberg@ki.se

From the ¹Department of Clinical Neuroscience, Karolinska Institute, Stockholm, Sweden; ²Department of Neuroradiology, Karolinska University Hospital, Stockholm, Sweden; ³A. A. Martinos Center for Biomedical Imaging, Department of Radiology, Massachusetts General Hospital, Boston, MA; ⁴Harvard Medical School, Boston, MA; ⁵NeuroPoly Lab, Institute of Biomedical Engineering, Polytechnique Montreal, Montreal, Quebec, Canada; ⁶Invicro, Boston, MA; ⁷Center for Medical Image Science and Visualization, Linköping University, Linköping, Sweden; ⁸SyntheticMR, Linköping, Sweden; ⁹Department of Medical Psychology, Karolinska University Hospital, Stockholm, Sweden; ¹⁰School of Engineering Sciences in Chemistry, Biology, and Health, Royal Institute of Technology, Stockholm, Sweden; and ¹¹Department of Neurology, Karolinska University Hospital, Stockholm, Sweden

Additional supporting information can be found in the online version of this article.

Multiple sclerosis (MS) is a chronic inflammatory and degenerative disease of the central nervous system and a leading cause of neurological disability in young adults.¹ The therapy for MS has been revolutionized in the past 2 decades, but available treatments have mainly focused on modifying the inflammatory disease activity.² New emerging treatments may promote remyelination, but studying their effects on the de- and remyelination dynamics in MS requires robust and clinically feasible ways to monitor the myelin content of the brain.^{3,4}

Magnetic resonance imaging (MRI) contributes to early diagnosis, optimized treatment monitoring, and more efficient clinical trials in MS.^{5,6} However, conventional MRI lacks specificity to myelin and is insensitive to diffuse MS pathology in normal-appearing tissue.⁶ Although the gold standard of myelin quantification is histopathological analysis postmortem, or rarely by in vivo tissue biopsy, innovations in MRI have allowed for noninvasive myelin quantification.^{7–10} Fast and robust noninvasive myelin quantification holds promise of being especially useful to study myelin dynamics in MS but also in other neurological disorders where myelin content is affected.¹⁰

In the myelin macrostructure, water is compartmentalized between the bilipid myelin sheaths. This myelin-bound water has strong magnetic interaction with the surrounding protons in the myelin macromolecules, which gives rise to distinctive MRI signal properties of the myelin-bound water with fast relaxation rates.⁷ Typically, myelin water imaging requires dedicated MRI sequences aiming to directly image the small pool of quickly relaxing myelin-bound water fraction with relatively long acquisition times and advanced data postprocessing.¹⁰ Although recent technological developments have led to faster imaging and improved robustness, they still require complex data analysis and lack US Food and Drug Administration (FDA) approval and/or CE marking for clinical application.¹⁰

A newly developed alternative myelin imaging technique is based on time-efficient and robust quantitative MRI for simultaneous T_1/T_2 relaxometry and proton density (PD) mapping that allows whole-brain coverage in 7 minutes.^{11,12} Based on these quantitative MRI measures, a myelin quantification technique has been developed called Rapid Estimation of Myelin for Diagnostic Imaging (REMyDI), which quantifies myelin based on the magnetization exchange from the water compartmentalized within the myelin sheath to the observable water pool.³ The methodology has been clinically approved, validated in forensic postmortem MRI,⁴ and shown to be more sensitive to MS lesions than the individual

relaxometry measures.¹³ The same acquisition can also be used to generate multiple image contrasts of diagnostic quality and robust brain volumetrics in MS, thus providing automated myelin quantification without additional scanning time.¹⁴ A systematic, combined clinical and histopathological validation of this new myelin imaging technique in MS is, however, warranted.

This study aimed to validate REMyDI *ex vivo* and apply it *in vivo* in MS, first by histopathological analysis in postmortem MS tissue to study its tissue specificity and then through scan–rescan repeatability measures in both healthy controls and MS patients. Finally, clinical application was done in a prospective cohort of healthy controls and MS patients with longitudinal clinical follow-up.

Patients and Methods

Ethical Considerations

This study, including both the *in vivo* and *ex vivo* aspects, was reviewed and approved by the respective local institutional review boards. Written informed consent was obtained for all *in vivo* participants. The *ex vivo* tissue samples were obtained by the Rocky Mountain Tissue Bank (Denver, CO) after informed consent. This study was conducted in accordance with the Declaration of Helsinki.

MRI Acquisition and Postprocessing

The quantitative MRI method used in this study is based on a single time-efficient multidynamic, multiecho acquisition. The technique has been described in detail previously.¹¹ In summary, a saturation-recovery sequence is applied with 2 echo times and 4 averages. For each average, the slice acquisition order is changed, which results in 4 different inversion times. Both the phase and magnitude data are saved, and the data are used to fit the curves for the longitudinal (R_1) and transversal (R_2) relaxation rates and to obtain the PD with background phase correction and a spin system simulation to compensate for the slice-selective radio-frequency pulse profile effects. This postprocessing was done automatically in seconds using SyMRI (version 11.0 beta 4 for Mac; Synthetic MR, Linköping, Sweden), producing quantitative R_1 , R_2 , and PD maps with correction for field inhomogeneities and partial volume effects.³

Myelin Quantification

The REMyDI myelin quantification is based on the R_1 , R_2 , and PD maps, where each voxel is modeled into 4 compartments—the myelin, cellular, free water, and excess parenchymal water partial volumes—as previously described.³ This is accomplished through a voxelwise

least-squares fit that models the relaxation behavior of the dominant slow-decay component of R_1 and R_2 while accounting for the amplitude of the PD signal.¹¹ The myelin partial volume has very fast relaxation rates and is not directly measurable but is instead estimated through its magnetization exchange and effect on the observable proton pool. The REMyDI myelin maps were generated automatically in SyMRI; representative examples are presented in Figure 1.

Ex Vivo Validation

Tissue Samples. Three coronal hemispheric sections were acquired from the Rocky Mountain Tissue Bank. All donors had been diagnosed with MS; there was a 71-year-old female donor diagnosed with secondary progressive MS (SPMS), a 46-year-old female donor diagnosed with SPMS, and a 56-year-old male donor diagnosed with SPMS. Anonymized clinical patient charts and autopsy reports were available for review along with clinical details and treatments, all of which are further summarized in Supplementary Table 1.

MRI Acquisition. The MS specimens were scanned at room temperature to ensure even temperature throughout the tissue. Scanning was performed on a Siemens Trio 3.0-T MRI scanner (Siemens Healthineers, Erlangen, Germany) with the aforementioned quantitative multiparametric

sequence.¹¹ A 32-channel head coil was used to obtain a high signal-to-noise ratio from the sample. To mitigate partial volume effects and facilitate registration with histology, this quantitative scan was acquired with high spatial resolution: coronal field of view of 180×144 mm, voxel size of $0.39 \times 0.39 \times 2.0$ mm, with a 0.75 distance factor, 15 slices, repetition time of 2,400 milliseconds, echo times of 25/101 milliseconds, flip angle of 120° for the saturation pulse, no acceleration, 6 averages, and total acquisition time of 32 minutes, 47 seconds. SyMRI was used to extract the R_1 , R_2 , and PD maps as described earlier. To compensate for the fixation and temperature effects, the R_1 and R_2 rates were rescaled by a factor of 3.3 and 1.9, respectively, based on correction factors available in the literature.¹⁵ SyMRI was also used to generate PD-weighted images (repetition time = 8,000 milliseconds, echo time = 10 milliseconds) for manual tissue segmentation, as described later.

Tissue Processing. Histopathological evaluation was conceptualized and executed by an experienced histotechnician (I.P.). Due to the challenges of acquiring and uniformly staining across whole-hemispheric tissue sections to match the MRI, optimization of the tissue processing was first performed on a bovine brain tissue sample of comparable size. The final optimized sectioning and staining techniques were then applied to the human tissue sample. Fiducial markers were added outside of the tissue for intersectional alignment and

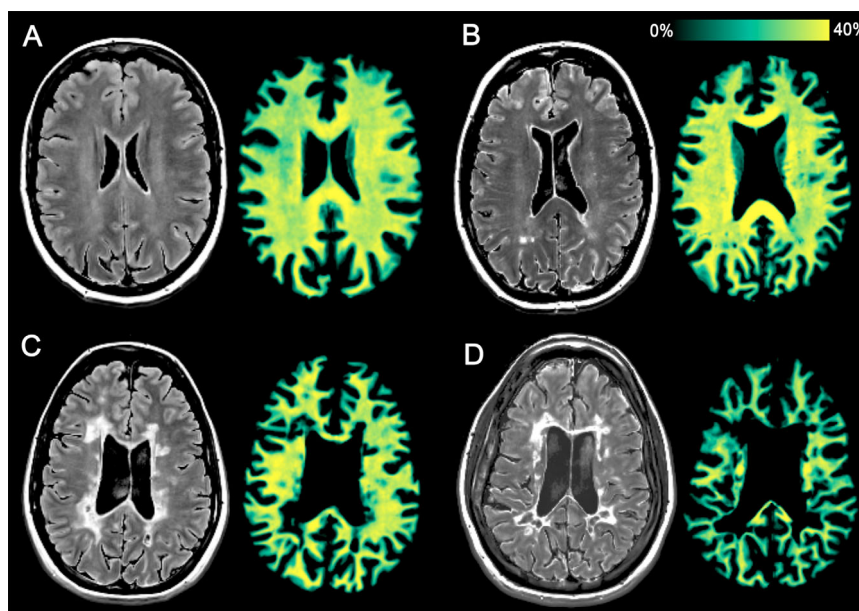


FIGURE 1: T_2 -weighted fluid-attenuated inversion recovery and the corresponding rapid myelin imaging in 4 representative study participants. (A) A 56-year-old female healthy control. (B) A 53-year-old female primary progressive multiple sclerosis patient, disease duration of 9 years, Expanded Disability Status Scale (EDSS) score of 3.5, Symbol Digit Modalities Test (SDMT) z score of -0.38 . (C) A 39-year-old female relapsing–remitting multiple sclerosis patient, disease duration of 14 years, EDSS score of 1.0, SDMT z score of -1.0 . (D) A 40-year-old female secondary progressive multiple sclerosis patient, disease duration of 25 years, EDSS of score 7.0, and SDMT z score of -3.9 .

registration purposes. Using a fully computerized cryomacrotome (CM3600 XP; Leica Biosystems, Wetzlar, Germany) operated at -18°C , $10\mu\text{m}$ -thick tissue slices were collected in groups of 5 slices at 13 levels with $150\mu\text{m}$ separation between levels through the whole sample and then transferred onto Kawamoto tape (Kawamoto, Osaka, Japan). Two myelin-specific stains (proteolipid protein-immunostaining and Luxol fast blue [Polysciences, Warrington, PA]) and an axonal stain (Bielschowsky silver) were then applied. Further details on the histopathological procedures are shown in Supplementary Table 1.

Histological Imaging. Each tissue section level was photographed, and white light images were balanced by contrast stretching to overcome any differences in color due to changes in lighting conditions. Each of the stained tissue sections was scanned using an Epson V600 scanner (4,800

dpi; $5.3 \times 5.3\mu\text{m}^2$ resolution), as shown in Figure 2. For each image, the optical density was calculated by transforming the color image to grayscale by taking the mean projection across color channels, to be as consistent as possible between the included histological stains. A 10-bin histogram of the optical density was then constructed for each combination of level and stain, with the range of the bins being the same for each image, with a range of 0 to 250.

MRI and Histological Comparative Analysis. Voxelwise analysis was chosen to compare the REMyDI and histological myelin quantification values across the whole coronal hemispherical samples. To facilitate accurate alignment of MRI and histological myelin measures, the MRI images of the samples were used to guide the histological sectioning by increments of $90\mu\text{m}$ until arrival at the MRI-corresponding depth. The PD-weighted image was used as a reference for the registration of the stained histological sections.

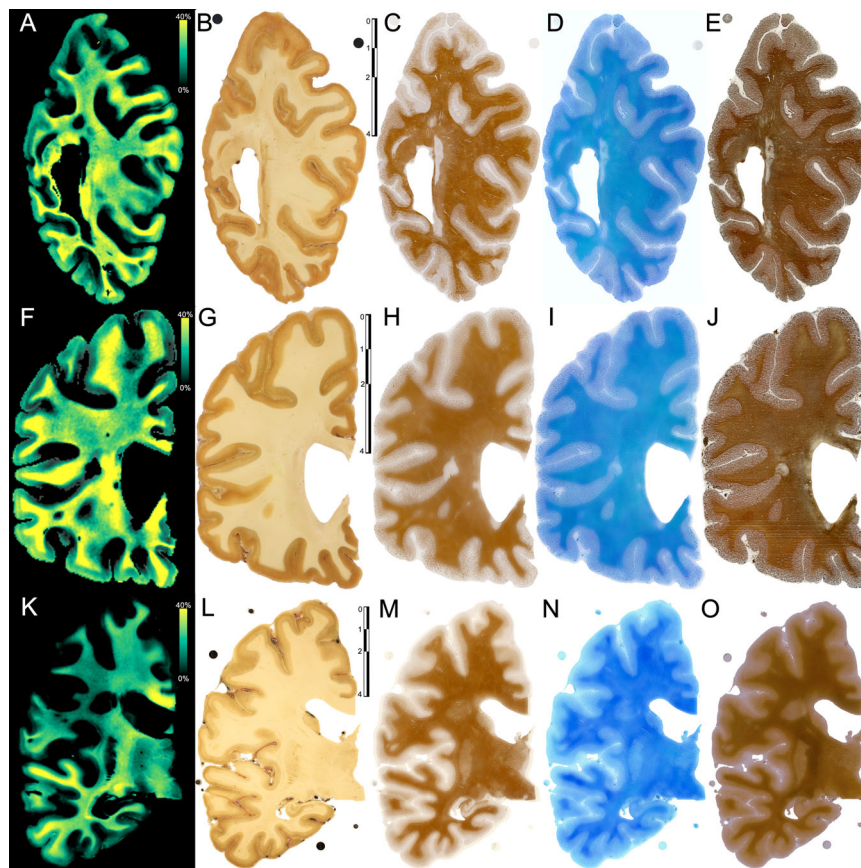


FIGURE 2: Ex vivo validation of Rapid Estimation of Myelin for Diagnostic Imaging (REMyDI) myelin quantification in multiple sclerosis. Whole-section coronal $10\mu\text{m}$ -thick tissue sections. Top row (A–E): Parietal coronal hemispheric brain tissue sample from a 71-year-old donor with secondary progressive multiple sclerosis (SPMS). Middle row (F–J): Frontal coronal hemispheric brain tissue sample from a 46-year-old donor with SPMS. Bottom row (K–O): Frontotemporal coronal hemispheric brain tissue sample from a 56-year-old donor with SPMS. First column (A, F, K): REMyDI myelin maps. Second column (B, G, L): Tissue samples before histological processing. Scale bars in centimeters. Third column (C, H, M): Proteolipid protein immunostaining. Fourth column (D, I, N): Luxol fast blue staining. Fifth column (E, J, O): Bielschowsky silver staining (some cutting artifacts can be appreciated in E and J).

The registration was carefully performed using ANTsRegistration (v2.1.0, ANTs, stnava.github.io/ANTs/)¹⁶ in 3 subsequent steps with the following parameters: rigid, affine (convergence = $100 \times 100 \times 100$, smoothing = $10 \times 5 \times 1$), and the symmetric image normalization method (nonlinear, convergence = 100×100 , smoothing = 1×0). The PD-weighted image was manually segmented into 4 tissue compartments—white matter, gray matter, lesions, and image artifacts—by a trained rater (R.O.), as illustrated in Figure 3. Artifacts in the MRI volume (accounting for 0.4% of the voxels) consisting of partial volume effects with vasculature, air bubbles, or cutting artifacts were excluded from the histological comparison.

In Vivo Repeatability and Clinical Validation

Participants and Clinical Assessments. In the prospective in vivo substudy, 71 patients diagnosed with MS according to the concurrent McDonald 2010 criteria¹⁷ were consecutively enrolled from the Department of Neurology at Karolinska University Hospital with a representation of all MS subtypes.¹⁸ For group-level comparison, we also included 21 age- and sex-matched controls. Predefined exclusion criteria were MRI contraindications, neurological comorbidities, or a history of head trauma; no participants were excluded. Physical disability in patients was assessed by a neurologist experienced in MS (S.F.) according to the Expanded Disability Status Scale (EDSS).¹⁹ Physical disability scores were available for all participants but one. The primarily recommended cognitive test in MS,²⁰ the Symbol Digit Modalities Test (SDMT), reflecting information processing speed, was assessed in 48 patients at baseline. Baseline clinical assessments were made within 6 months of the MRI acquisition. Longitudinal clinical assessments were additionally performed for both EDSS ($n = 70$) and SDMT ($n = 32$), with a mean follow-up time of 2.0 ± 0.8 years and 1.5 ± 0.4 years, respectively. SDMT test scores were converted into z scores with regard to age and sex, based on normative data.²¹ The demography of the participants is detailed in Table 1, with the disease modifying therapies shown in Supplementary Table 2.

MRI Acquisition. The same scanner, model, software, and sequence used ex vivo were then applied in vivo. A 12-channel head coil was used in vivo because it was routinely applied in the clinical MS protocol and allowed for large head sizes. Imaging parameters were axial field of view of 230×184 mm, voxel size of $0.9 \times 0.9 \times 3.0$ mm³ with a 0.5 distance factor, 30 to 34 slices (to ensure full intracranial coverage), repetition time of 4,260 milliseconds, echo times of 22/100 milliseconds, effective inversion times of 150/580/2,000/4,130 milliseconds, flip angle of 120° for

the saturation pulse, generalized auto-calibrating partially parallel acquisitions acceleration factor 2, and a total acquisition time of 6 minutes, 50 seconds to 7 minutes, 47 seconds (depending on the number of slices needed for full intracranial coverage). SyMRI was used to generate the quantitative maps, REMyDI, T₁-weighted images (repetition time = 500 milliseconds, echo time = 10 milliseconds), and T₂-weighted fluid inversion recovery images (repetition time = 15,000 milliseconds, echo time = 100 milliseconds, inversion time = 3,000 milliseconds).

MRI Repeatability. To study the robustness of the myelin quantification, 13 patients and 19 controls were scanned twice with the same sequence after repositioning. The demography of the repeatability cohort is described in Table 2. The variability of the myelin measurements across the whole tissue volume was assessed by calculating the coefficient of variation between the 2 scans:

$$\frac{\text{Standard Deviation } (\sigma)}{\text{Mean } (\mu)} \times 100$$

MRI Volumetry. The quantitative maps in SyMRI were also used to calculate the intracranial volume.^{14,22} Representative examples of the in vivo T₂-weighted fluid-attenuated inversion recovery images and myelin quantification maps are provided in Figure 1. To extract the myelin content specifically in normal-appearing gray matter (NAGM) and white matter (NAWM), semimanual segmentations were performed. The T₁-weighted images were segmented using Statistical Parametric Mapping 12 (<http://www.fil.ion.ucl.ac.uk/spm/software/spm12>; University College London, London, UK)²³ to obtain probabilistic maps of the gray matter and white matter. T₂-weighted fluid-attenuated inversion recovery images were used to perform probabilistic segmentation of MS lesions in Lesion Segmentation Tool (version 2.0.15; Technical University of Munich, Munich, Germany, <https://www.applied-statistics.de/lst.html>).²⁴ The probabilistic masks were binarized using FMRIB Software Library (version 5.0; Oxford University, Oxford, United Kingdom, fsl.fmrib.ox.ac.uk/fsl)²⁵ using a 0.5 threshold and then manually corrected by trained raters (R.O. and M.P.) and finally reviewed by an experienced rater (T.G.). The manual edits were performed in ITK-SNAP (version 3.6.0; University of Pennsylvania, Philadelphia, PA, itksnap.org).²⁶ The lesion masks were used to remove lesioned voxels from the gray and white matter segmentations, resulting in masks of the NAGM and NAWM. These masks were then applied to the REMyDI maps to extract the myelin volume for these tissues and normalized to the intracranial volume to obtain the NAGM and

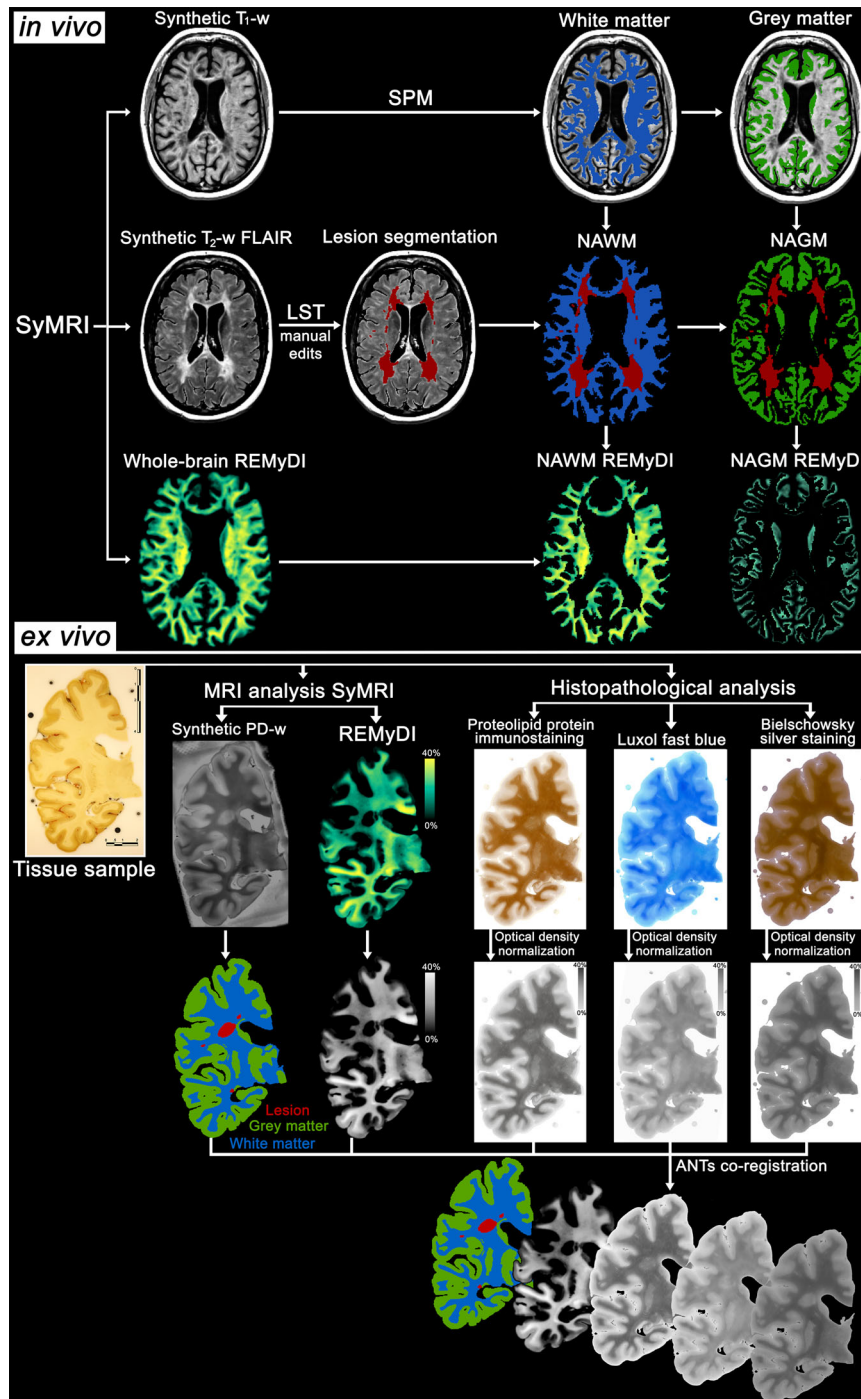


FIGURE 3: Overview of the image acquisition and processing pipeline. In vivo image processing: SyMRI T₁-weighted, T₂-weighted fluid-attenuated inversion recovery (FLAIR) images, and Rapid Estimation of Myelin for Diagnostic Imaging (REMyDI) processed for tissue segmentation, lesion masks, and normal-appearing white (NAWM) and gray matter (NAGM) volumes and myelin fractions. Example from a 50-year-old relapsing–remitting multiple sclerosis patient with 24-year disease duration, an Expanded Disability Status Scale score of 3.0, and Symbol Digit Modalities Test z score of –2.4. Ex vivo image processing: The coronal frontotemporal multiple sclerosis tissue sample was similarly scanned to obtain proton density (PD)-weighted images for tissue segmentation and REMyDI for myelin quantification. The sample was then histopathologically processed and stained using proteolipid protein immunostaining, Luxol fast blue, and Bielschowsky silver staining. Magnetic resonance imaging (MRI) and histologically stained sections were registered by ANTsRegistration. Scale bar shown in centimeters. ANTs = Advanced Normalization Tools; LST = Lesion Segmentation Tool; SPM = statistical parametric mapping; w = weighted images.

TABLE 1. Participant Demography and MRI Metrics

	MS Patients				
	Healthy Controls	All MS	RRMS	SPMS	PPMS
Demography					
Participants, n	21	71	53	15	3
Female/male, n	12/9; $p = 0.43^a$	49/22	39/14	8/7	2/1
Age, yr	35.9 ± 13.8; $p = 0.14^b$	40.9 ± 10.2	38.3 ± 10.1	46.9 ± 4.3	56.5 ± 7.8
Disease duration, yr	N/A	12.2 ± 8.4	10.0 ± 7.2	20.9 ± 7.4	7.9 ± 4.0
EDSS					
Baseline score, median (n)	N/A	2.0 ± 2.0 (70)	1.5 ± 1.0 (53)	3.75 ± 3.3 (14)	3.5 ± 3.0 (3)
Follow-up score, median (n)	N/A	2.0 ± 2.1 (70)	1.5 ± 1.5 (53)	5.0 ± 3.3 (14)	6.0 ± 2.0 (3)
Follow-up time, yr	N/A	2.0 ± 0.8	1.9 ± 0.8	2.2 ± 0.8	1.7 ± 1.1
SDMT					
Baseline z score (n)	N/A	-1.3 ± 1.2 (49)	-1.1 ± 1.1 (37)	-2.1 ± 1.2 (10)	-0.7 ± 0.4 (2)
Follow-up z score (n)	N/A	-1.2 ± 0.9 (32)	-1.2 ± 0.9 (26)	-1.4 ± 0.9 (4)	-0.1 ± 0.6 (2)
Follow-up time, yr	N/A	1.5 ± 0.5	1.6 ± 0.4	1.7 ± 0.5	0.7 ± 0.1
Conventional MRI metrics					
Lesion volume, ml, median	N/A	9.1 ± 18	6.4 ± 16 $p = 0.002^{c,d}$ vs SPMS	18.2 ± 47	4.6 ± N/A
NAWM fraction, %	27.1 ± 1.9 $p = 0.001^{b,d}$ vs all MS	25.1 ± 3.2	25.4 ± 2.8 $p = 0.004^{b,d}$ vs HC $p = 0.27^b$ vs SPMS	24.1 ± 4.3 $p = 0.019^{b,d}$ vs HC	24.9 ± 0.4
NAGM fraction, %	40.5 ± 3.1 $p = 0.53^b$ vs all MS	39.0 ± 3.4	39.7 ± 3.0 $p = 0.28^b$ vs HC $p = 0.018^{b,d}$ vs SPMS	37.0 ± 3.6 $p = 0.005^{b,d}$ vs HC	36.0 ± 2.8
MRI myelin quantification					
Whole-brain myelin fraction, % ^c	12.6 ± 0.9 $p = 0.004^{b,d}$ vs all MS	11.8 ± 1.6	12.0 ± 1.4 $p = 0.026^{b,d}$ vs HC $p = 0.13^b$ vs SPMS	11.1 ± 2.0 $p = 0.014^{b,d}$ vs HC	12.3 ± 0.1
NAGM myelin fraction, % ^c	1.72 ± 0.1 $p = 0.67^b$ vs all MS	1.71 ± 0.1	1.72 ± 0.1 $p = 0.95^b$ vs HC $p = 0.061^b$ vs SPMS	1.63 ± 0.2 $p = 0.083^b$ vs HC	1.77 ± 0.1
NAWM myelin fraction, % ^c	10.6 ± 1.0 $p = 0.001^{b,d}$ vs all MS	9.6 ± 1.7	9.8 ± 1.5 $p = 0.009^{b,d}$ vs HC $p = 0.15^b$ vs SPMS	8.9 ± 2.1 $p = 0.010^{b,d}$ vs HC	10.1 ± 0.1

All values are given as mean ± standard deviation unless otherwise specified. Medians are reported with ± the interquartile range.

^aBy χ^2 test (2-tailed).

^bBy unpaired t test (2-tailed, equal variances not assumed).

^cBy Mann–Whitney U test (2-tailed, equal variances not assumed).

^dProbability value remained significant after correction for multiple comparison.

^eAll myelin fractions are given as percent after normalization to the intracranial volume.

EDSS = Expanded Disability Status Scale; HC = healthy controls; MRI = magnetic resonance imaging; MS = multiple sclerosis; N/A = not applicable; NAGM = normal-appearing gray matter; NAWM = normal-appearing white matter; PPMS = primary progressive multiple sclerosis; RRMS = relapsing–remitting multiple sclerosis; SDMT = Symbol Digit Modalities Test; SPMS = secondary progressive multiple sclerosis.

TABLE 2. Demography and Coefficient of Variation Results for the Repeatability Subcohort

	All Participants	Healthy Controls	MS Patients
Demography			
Participants, n	32	19	13
Female/male, n	22/10	10/9 ^a	11/2
Age, yr	37.5 ± 13.5	37.1 ± 14.1 ^b	38.2 ± 13.2
Disease duration, yr	N/A	N/A	13.0 ± 10.6
Whole-brain myelin fraction			
Coefficient of variation, %			
Mean	1.2 ± 1.5	1.4 ± 1.8	0.82 ± 0.75
Median	0.58, 0.0–6.5	0.58, 0.0–6.5	0.68, 0.0–2.6
NAWM myelin fraction			
Coefficient of variation, %			
Mean	0.52 ± 0.63	0.58 ± 0.73	0.42 ± 0.46
Median	0.29, 0.0–3.0	0.38, 0.0–3.0	0.24, 0.1–1.8
NAGM myelin fraction			
Coefficient of variation, %			
Mean	1.1 ± 0.81	1.1 ± 0.90	1.1 ± 0.69
Median	0.87, 0.0–2.9	0.73, 0.0–2.9	1.1, 0.2–2.5

All values representing the coefficient of variation are in percent and provided as mean ± standard deviation followed by median, range. For NAWM and NAGM myelin fraction repeatability data, it was not possible to extract for 1 MS patient and 2 healthy controls due to image postprocessing errors.

^a $P = 0.061$ versus MS patients by χ^2 test (2-tailed).

^b $P = 0.83$ versus MS patients by unpaired t test (2-tailed, equal variances not assumed).

MS = multiple sclerosis; N/A = not applicable; NAGM = normal-appearing gray matter; NAWM = normal-appearing white matter.

NAWM myelin fractions. The image analysis pipeline is further described in Figure 3.

Statistical Analysis

All statistical analyses were performed with IBM SPSS Statistics version 25 for Mac (IBM, Armonk, NY). Normality was determined by the Shapiro–Wilk test, histogram analysis, and ensuring both the skewness and kurtosis values were within a range of ± 1 . Group-level comparisons for parametric variables were compared using the independent sample t test (equal variance not assumed), and nonparametric variables were done using the independent samples Mann–Whitney U test (both 2-tailed). Bivariate correlations between parametric variables were calculated using Pearson correlation and Spearman correlation for nonparametric data. Sex differences between patients and controls were assessed by a

χ^2 test (2-tailed). Voxelwise comparison of histology and REMyDI myelin content was done using Pearson correlation. Individual stepwise linear regressions with the clinical disability metrics as the dependent variable were accomplished by transforming the nonparametric variables (EDSS by \log_{10} transformation and lesion fraction by square root transformation). A threshold of $p < 0.05$ was considered statistically significant. False discovery rate correction for multiple comparisons was applied for each of the 2 clinical disability measurements across the corresponding baseline, longitudinal and corrected comparisons.²⁷

Results

Ex Vivo MRI Histological Correlations

The REMyDI myelin quantification correlated ($p < 0.001$ for all) with both of the myelin-specific histological staining

methods across the entire samples: proteolipid protein immunostaining ($r = -0.73$, $r = -0.63$, $r = -0.66$) and Luxol fast blue ($r = -0.66$, $r = -0.61$, $r = -0.63$), demonstrated in Figure 4. Generally, the correlations to the axonal Bielschowsky silver staining ($r = -0.58$, $r = -0.48$, $r = -0.63$; all $p < 0.001$) were numerically lower. The histological myelin staining methods were also highly correlated with one another (proteolipid protein immunostaining vs Luxol fast blue: $r = 0.92$, $r = 0.93$, $r = 0.91$). Individual quantitative maps (PD, R_1 , and R_2) demonstrated a nonlinear relationship with myelin histology, suggesting that other factors influence the R_1 and R_2 maps and therefore cannot alone sufficiently approximate myelin content. The PD demonstrated a linear relationship, although to a lower degree than that of REMyDI. The PD, R_1 , and R_2 and histological

voxelwise correlations are shown in further detail in Supplementary Table 3.

In Vivo Repeatability

The whole-brain REMyDI myelin fraction was robust, with an overall mean coefficient of variance of $1.2 \pm 1.5\%$ (median = 0.58%, range = 0.0–6.5%). In the MS cohort, the mean coefficient of variation was $0.82 \pm 0.75\%$ (median = 0.68%, range = 0.0–2.6%). In healthy controls, the overall mean coefficient of variance was $1.4 \pm 1.8\%$ (median = 0.58%, range = 0.0–6.5%). The overall myelin fractions in the NAWM and NAGM were also found to be robust, with a mean coefficient of variance of $0.52 \pm 0.63\%$ (median = 0.29%, range = 0–3.0%) and $1.1 \pm 0.81\%$ (median = 0.87%, range = 0–2.9%), respectively. The demography and myelin

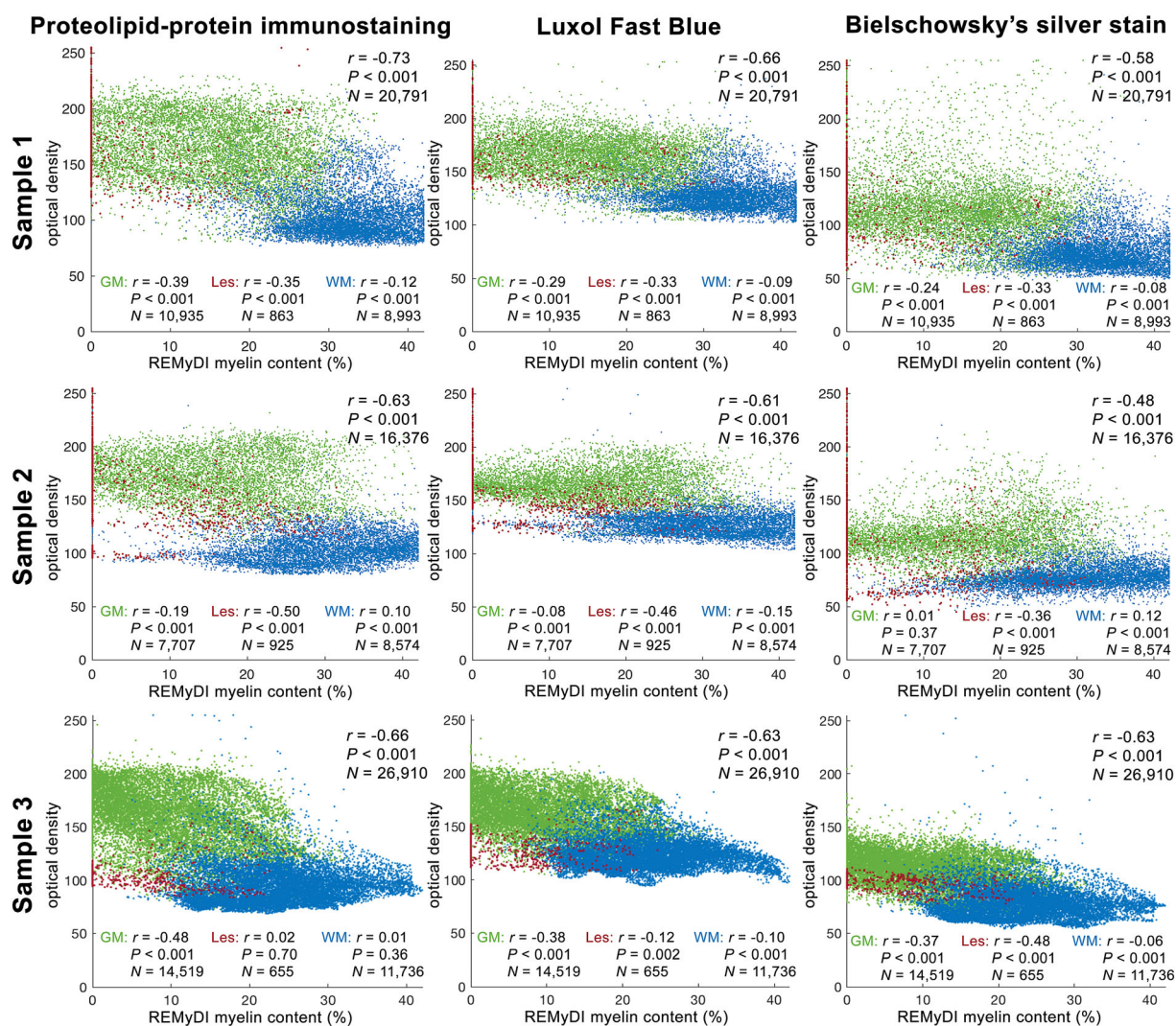


FIGURE 4: Comparative correlations of individual Rapid Estimation of Myelin for Diagnostic Imaging (REMyDI) myelin quantification with myelin-specific histopathological stainings. Three multiple sclerosis brain tissue samples' voxelwise Pearson correlations of the REMyDI myelin maps with the histological stain uptake optical densities for proteolipid protein immunostaining, Luxol fast blue, and Bielschowsky silver staining. Tissue segmentation is identified as gray matter (GM) in green, white matter (WM) in blue, and lesions (Les) in red, alongside the respective tissue voxel count (N).

quantification results for the repeatability cohort are reported in Table 2.

In Vivo Group Comparison

The tissue-specific *in vivo* REMyDI values in MS subjects, across subtypes, and healthy controls are listed in Table 1. There was no significant difference in age or sex between patients and controls. There was no significant difference between males and females in any of the conventional or REMyDI myelin quantification MRI metrics across all participants or within the control/MS subgroups. Relative to controls, MS patients had lower myelin fractions in the whole brain and NAWM. Relapsing–remitting MS patients had lower whole-brain and NAWM myelin fractions than controls. SPMS patients also had lower whole-brain and NAWM myelin fractions than controls. There was a trend of lower REMyDI myelin values in the NAGM of SPMS patients compared to relapsing–remitting MS patients.

In Vivo Clinical Correlations

Regarding physical disability, the whole-brain and NAWM myelin content as well as the lesion volume fraction correlated with baseline EDSS scores. The same MRI metrics, along with the NAWM volume fraction, correlated with EDSS scores at 2-year clinical follow-up. However, after correcting for baseline EDSS, only the myelin content in the whole brain and NAWM were significantly correlated with longitudinal EDSS. Linear regression identified that baseline EDSS was most strongly influenced by the lesion fraction, but at 2-year follow-up, whole-brain myelin fraction was found to be the strongest contributor.

In terms of cognitive disability, whole-brain and NAWM myelin content as well as the NAWM volume fraction correlated with baseline SDMT scores. The NAGM myelin content tended to be correlated with longitudinal SDMT scores at 1.5-year follow-up, even after correcting for baseline SDMT, although it did not survive correction for multiple comparisons. Stepwise linear regression identified the baseline SDMT score was most strongly related with whole-brain myelin fraction and, longitudinally, mostly associated with a combination of whole-brain and NAGM myelin fractions. Full numerical description of the baseline and longitudinal clinical correlations with REMyDI can be found in Table 3; similarly, linear regression results are detailed in Figure 5.

Discussion

In this study, we aimed to validate REMyDI, a new rapid MRI-based method for myelin quantification, in MS. First, we performed *ex vivo* validation by histopathological staining. Second, we performed *in vivo* validation by evaluating the

robustness by repeated scanning with repositioning and through clinical application in healthy controls and MS patients followed clinically over time. We found that REMyDI correlated with myelin stains, was robust in patients and controls, and showed clinically interesting cross-sectional and longitudinal associations to cognitive and physical disability in MS.

Although there are several available myelin imaging techniques, they have yet to make their way into clinical practice due to practical limitations of the techniques in regard to acquisition time, complexity of postprocessing, or lack of clinical approval (US FDA clearance and/or CE marked).¹⁰ We will discuss our findings relative to prominent myelin imaging techniques, primarily those with contextual comparison, having been histopathologically validated in humans and applied clinically in the brain of adult MS patients.

Ex Vivo Validation

Different staining methods have been used in previous MRI histological validation studies of myelin imaging. Multicomponent T₂ relaxometry at 1.5 T ($r^2 = 0.67$)²⁸ and 7 T ($r^2 = 0.78$),⁸ magnetization transfer ratio ($r = -0.84$),²⁹ and macromolecular proton fraction ($r = -0.80$)³⁰ have all shown strong correlations with Luxol fast blue in fixed human MS brain tissue samples. The correlation of REMyDI to Luxol fast blue in our study ($r = -0.66$, $r = -0.61$, $r = -0.63$) is comparably more moderate, although direct comparisons between studies are complicated by methodological differences. In the current study, proteolipid protein immunostaining had the highest correlation with REMyDI, albeit with a small margin. Proteolipid protein immunohistochemical staining has previously been applied to study cortical demyelination with a T₁/T₂-weighted ratio.³¹ However, the T₁/T₂-weighted ratio has come under scrutiny having been shown to be more strongly associated with dendrite density than myelin content within the cortex.^{12,32} In this study, the associations of REMyDI myelin quantification with the myelin stains were generally numerically higher than with the axonal stain, suggesting that REMyDI is more reflective of myelin content than axons. However, axon-related and myelin-related stains are expected to be highly correlated due to the colocalization of myelin around the axons as well as the concomitant processes of demyelination and axonal loss. In contrast to previous *ex vivo* studies, we have chosen to compare the MRI-based and histological myelin quantifications using a whole-sample voxelwise approach, rather than manual regions of interest, to avoid manual selection bias and thereby objectively report the correlation for all of the voxels/pixels. Furthermore, previous histopathological analyses have selected multiple small tissue sections (~1 cm³) taken from a larger sample and processed individually. This approach may

TABLE 3. Clinical Correlations of the Brain Volumetrics and Myelin Quantification

	Expanded Disability Status Scale						Symbol Digit Modalities Test					
	Baseline, n = 70		Follow-up, n = 70		Corrected Follow-up, n = 70		Baseline, n = 49		Follow-up, n = 32		Corrected Follow-up, n = 28	
	ρ	p	ρ	p	ρ	p	r/ρ	p	r/ρ	p	r/ρ	p
REMyDI myelin content												
Brain	-0.26 ^a	0.032 ^{a,b}	-0.41 ^a	<0.001 ^a	-0.30 ^a	0.013 ^a	0.56 ^a	<0.001 ^a	0.33	0.069	0.04	0.82
NAGM	-0.08	0.50	0.04	0.77	0.18	0.14	0.09	0.54	0.38 ^a	0.034 ^{a,b}	0.45 ^a	0.014 ^{a,b}
NAWM	-0.26 ^a	0.032 ^{a,b}	-0.41 ^a	<0.001 ^a	-0.30 ^a	0.011 ^a	0.54 ^a	<0.001 ^a	0.28	0.12	-0.007	0.97
Conventional MRI metrics												
Lesion fraction	0.36 ^a	0.002 ^a	0.40 ^a	<0.001 ^a	0.23	0.063	-0.27	0.060	-0.24	0.18	-0.25	0.19
NAGM fraction	-0.19	0.13	-0.19	0.11	-0.20	0.10	0.18	0.21	0.16	0.38	0.15	0.43
NAWM fraction	-0.19	0.11	-0.32 ^a	0.008 ^a	-0.21	0.079	0.42 ^a	0.003 ^a	0.30	0.19	0.18	0.35

^a $p < 0.05$.
^bThe p value was nonsignificant after correcting for multiple comparisons.
MRI = magnetic resonance imaging; NAGM = normal-appearing gray matter; NAWM = normal-appearing white matter; REMyDI = rapid estimation of myelin for diagnostic imaging.

potentially introduce differences in myelin stain uptake between the individual samples.

In Vivo Repeatability

To monitor the myelin content in patients across time and to evaluate the potential remyelinating effects of treatment, it is essential to have a reliable and robust method. We have shown, through scan–rescan with repositioning, that REMyDI is highly reproducible with a low mean coefficient of variance in both healthy controls and MS patients. Our repeatability results are in line with a technically oriented study of REMyDI with 10 healthy controls scanned on three 3-T scanners from different vendors with high reproducibility ($r^2 = 0.999$).³³ The robustness of REMyDI is likely because the technique is not solely based on a single parameter but rather on simultaneous T_1 and T_2 relaxometry and PD mapping with automatic correction for magnetic field inhomogeneities, reducing the scanner variation effect and B_1 -field imperfections. Only some of the most established myelin imaging techniques have undergone precision studies¹⁰; the foremost of these is multicomponent T_2 relaxometry, where early studies have found mean scan–rescan coefficients of variance of 19% in 5 MS patients^{9,34} and 4.0% (range = 0.2–25%)⁹ using an 18-minute 3-dimensional version on 5 healthy volunteers. Two later versions of the technique decreased the acquisition time to ~4 minutes by increasing the voxel size^{9,35} to 28mm³ or halving the number

of echoes³⁶ to find respective mean coefficient of variance of 12% (range = 4–25%) in 6 healthy volunteers³⁵ and coefficient of variances ranging from 1.3 to 2.4% within 5 white matter regions of interest in 11 healthy volunteers.³⁶ The multicomponent driven equilibrium single pulse observation of T_1 and T_2 (mcDESPOT) myelin water method has shown whole-brain mean coefficients of variation of 7.9% (range = 7.2–9.3%) and 6.4% (range = 5.4–7.1%), for T_2 and T_1 respectively, in 7 healthy volunteers at 1.5 T in 12 minutes.^{9,37} Followed by a study of 7 controls to find 3.8% in white matter and 7.9% in gray matter using a ~14-minute sequence.³⁸ The introduction of a third non-exchanging water pool in mcDESPOT led to more robust myelin estimation in 4 brain regions of healthy volunteers, with a mean coefficient of variation of 5.9% (range = 5.1–6.4%).³⁹ In comparison with the evaluations of other myelin imaging techniques, the median coefficient of variance of REMyDI (0.58%, range = 0.0–6.5%) is comparably very robust.

In Vivo Clinical Applications

This study found lower myelin fractions in both the whole brain and NAWM of relapsing–remitting and secondary progressive MS patients relative to healthy controls. The finding of low NAWM myelin content suggests that REMyDI is able to detect diffuse demyelination. A sensitive myelin marker such as this is likely to be clinically relevant,⁶ which is

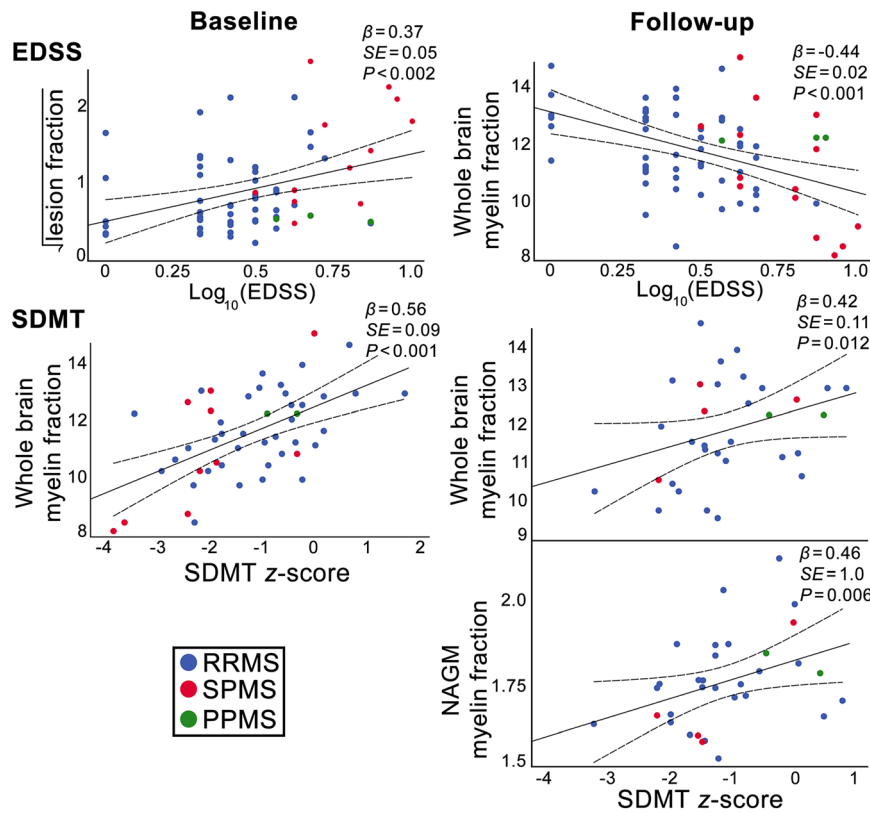


FIGURE 5: Linear regression of the clinical disability metrics with the magnetic resonance imaging metrics. Expanded Disability Status Scale (EDSS) scores were best characterized by the lesions fraction at baseline ($R^2 = 0.14$, $F = 10.7$, $p < 0.002$) and the whole-brain Rapid Estimation of Myelin for Diagnostic Imaging (REMyDI) myelin fraction at follow-up ($R^2 = 0.20$, $F = 16.5$, $p < 0.001$). SDMT scores at baseline was also best characterized by the whole-brain REMyDI myelin fraction ($R^2 = 0.32$, $F = 21.8$, $p < 0.001$). Symbol Digit Modalities Test (SDMT) at follow-up was best described by a combination of REMyDI myelin fraction in the whole brain and in the normal-appearing gray matter (NAGM; $R^2 = 0.31$, $F = 6.6$, $p = 0.004$). For the purpose of linear regression, EDSS was treated as a continuous variable and was \log_{10} transformed and normalized lesion fraction by the square root to become approximately normally distributed. Relapsing-remitting multiple sclerosis (RRMS) patients shown in blue, secondary progressive multiple sclerosis (SPMS) in red, and primary progressive multiple sclerosis (PPMS) in green. SE = standard error.

supported by our findings of associations with both cognitive and physical disability. Baseline and 2-year longitudinal follow-up of physical disability showed significant correlations with myelin quantification in the whole brain and NAWM, comparable to that of conventional MRI metrics. Cognitive disability in patients at baseline showed correlation with whole-brain and NAWM myelin fractions more prominently than conventional MRI metrics. Cognitive impairment is traditionally associated with conventional MRI metrics of lesion accumulation and atrophy,^{38,41} whereas this study has also highlighted diffuse demyelination as a significant contributor to an individual's cognitive status. Linear regression identified whole-brain myelin fraction to be most singularly related to clinical disability, suggesting that rapid myelin imaging provides a valuable component in describing an individual patient's physical and cognitive disability profile.

Our results are in line with clinical applications of previous myelin imaging techniques in MS. Multicomponent T_2

relaxometry was first to identify NAWM demyelination^{42,43} and monitor treatment response in MS.⁴³ Clinically, mcDESPOT has been applied to evaluate demyelination and physical disability in 17 primary progressive MS (PPMS) patients using a ~14-minute sequence, finding significant correlations ($r = 0.58$, $p = 0.008$) between the myelin water fraction and worsening EDSS scores.⁴⁴ The same technique at 10 minutes found lower myelination in 15 PPMS patients' NAWM compared to controls; however, no significant correlation between the NAWM myelin content and clinical physical disability was found.⁴⁵ Magnetization transfer ratio⁴⁶ correlated with cognitive disability in SPMS patients' NAGM ($r = 0.46$, $p < 0.0001$) and NAWM ($r = 0.33$, $p < 0.0001$) but not with EDSS.⁴⁷ Inhomogeneous magnetization transfer ratio⁴⁸ in white matter structures correlated with physical disability.⁴⁹ Lastly, the T_1/T_2 -weighted ratio has recently been applied clinically to found differences in the cortex and in the white matter of MS patients compared to controls,⁵⁰

but its specificity to myelin, primarily in white matter, has been questioned.^{12,32,51} In addition, the inclusion of the “excess parenchymal water” compartment allows the REMyDI model to account for the presence of the concurrent edema³ that is associated with MS lesions,¹ which can confound other myelin imaging methods.⁵²

Limitations of the Study

For the ex vivo comparison, only 3 samples were analyzed due to the limited availability of large MS tissue samples and the costly and complex histological evaluation. We partly compensated for the low sample size by maximizing the usefulness of the sample by performing multiple staining protocols and analyzing across all voxels of the sample rather than manually selecting regions of interest. Although the MRI sequence and postprocessing remained conceptually the same in vivo and ex vivo, it was necessary to compensate for the temperature and effects of fixation ex vivo and rescale the relaxation maps based on the correction factors provided by Birkl and colleagues.¹⁵ Cognitive testing was only performed in about two-thirds of the patients, and there was also some longitudinal drop out. However, the subcohort for which cognitive testing was available remained a clinically representative cohort of MS patients.¹⁸

Future Considerations

From a clinical perspective, the next step is to perform longitudinal REMyDI measurements to study the dynamics of demyelination versus remyelination in conjunction with disability metrics in MS. Future studies with larger sample sizes should try to discern differences in the demyelinating pathology in different MS phenotypes. Comparing demyelination in different structures and their relative contribution to clinical disability would also be of clinical interest. REMyDI could also be suited to monitor demyelination in other disorders, such as neuromyelitis optica, acute disseminated encephalomyelitis, leukodystrophies, developmental disorders, stroke, and primary neurodegenerative conditions.⁵² From a technical standpoint, further studies can assess the effect that iron accumulation in MS has on the T₂ signal and the REMyDI model. Direct comparison of REMyDI with other myelin imaging techniques would also be valuable.

In summary, this study demonstrates that REMyDI, a new rapid myelin imaging technique, correlates well with myelin stainings and produces robust in vivo myelin quantification that is related to clinical disability measures in patients with MS both at baseline and follow-up. Clinical applications revealed high sensitivity to both focal and diffuse demyelination in MS. This suggests that REMyDI,

which has been approved for clinical use, is suitable for detecting demyelination in MS and is thus a promising technique to monitor the dynamic demyelination and remyelination processes throughout the clinical course of MS. This technique may also prove to be useful for other pathologies affecting the myelin and a suitable quantitative imaging biomarker for treatment studies aimed at enhancing remyelination.

Acknowledgment

This study was funded by Stockholm Region and Karolinska Institutet (ALF grants 20120213, 20150166, 20170036, CIMED junior grant 20190565); MultipleMS (EU Horizon 2020 grant 733161; R.O.) and COMBAT-MS (Patient-Centered Outcomes Research Institute grant MS-1511-33196; R.O.); and the Swedish Society for Medical Research and the Christer Lindgren and Eva Fredholm Foundation (T.G.).

We thank the participants for making this study possible and the Rocky Mountain MS Center Tissue Bank and the MS patients and their family for their tissue donation to further our understanding of the disease. We also thank the MRI staff at Karolinska University Hospital and V. Barletta for their help with data acquisition, A. Varjabedian and A. van der Kouwe for helpful advice on ex vivo imaging procedures, and A. Lukose for valuable comments on the manuscript.

Author Contributions

R.O., I.P., M.W., M.U., C.A.T., F.P., M.K.W., C.M., and T.G. contributed to the conception and design of the study. R.O., G.M., I.P., M.W., Y.F., Å.B., M.P., C.A.T., J.C.A., S.F., C.M., and T.G. contributed to the acquisition and analysis of data. R.O. and T.G. contributed to drafting the manuscript and preparing the figures.

Potential Conflicts of Interest

M.W.: Employment, stock/stock options, SyntheticMR AB (SyMRI software). All the remaining authors have nothing to report.

References

- Dutta R, Trapp BD. Mechanisms of neuronal dysfunction and degeneration in multiple sclerosis. *Prog Neurobiol* 2011;93:1–12.
- Ransohoff RM, Hafler DA, Lucchinetti CF. Multiple sclerosis—a quiet revolution. *Nat Rev Neurol* 2015;11:134–142.
- Warntjes M, Engström M, Tisell A, Lundberg P. Modeling the presence of myelin and edema in the brain based on multi-parametric quantitative MRI. *Front Neurol* 2016;7:16.

4. Wamntjes JBM, Persson A, Berge J, Zech W. Myelin detection using rapid quantitative MR imaging correlated to macroscopically registered Luxol fast blue-stained brain specimens. *Am J Neuroradiol* 2017;38:1096–1102.
5. Wattjes MP, Rovira À, Miller D, et al. Evidence-based guidelines: MAGNIMS consensus guidelines on the use of MRI in multiple sclerosis—establishing disease prognosis and monitoring patients. *Nat Rev Neurol* 2015;11:597–606.
6. Enzinger C, Barkhof F, Ciccarelli O, et al. Nonconventional MRI and microstructural cerebral changes in multiple sclerosis. *Nat Rev Neurol* 2015;11:676–686.
7. Laule C, Vavasour IM, Kolind SH, et al. Magnetic resonance imaging of myelin. *Neurotherapeutics* 2007;4:460–484.
8. Laule C, Kozlowski P, Leung E, et al. Myelin water imaging of multiple sclerosis at 7 T: correlations with histopathology. *Neuroimage* 2008;40:1575–1580.
9. Meyers SM, Vavasour IM, Mädler B, et al. Multicenter measurements of myelin water fraction and geometric mean T2: intra- and intersite reproducibility. *J Magn Reson Imaging* 2013;38:1445–1453.
10. Alonso-Ortiz E, Levesque IR, Pike GB. MRI-based myelin water imaging: a technical review. *Magn Reson Med* 2015;73:70–81.
11. Wamntjes JBM, Leinhard OD, West J, Lundberg P. Rapid magnetic resonance quantification on the brain: optimization for clinical usage. *Magn Reson Med* 2008;60:320–329.
12. Hagiwara A, Hori M, Kamagata K, et al. Myelin measurement: comparison between simultaneous tissue relaxometry, magnetization transfer saturation index, and T1w/T2w ratio methods. *Sci Rep* 2018; 8:10554.
13. Hagiwara A, Hori M, Yokoyama K, et al. Utility of a multiparametric quantitative MRI model that assesses myelin and edema for evaluating plaques, periplaque white matter, and normal-appearing white matter in patients with multiple sclerosis: a feasibility study. *Am J Neuroradiol* 2017;38:237–242.
14. Granberg T, Uppman M, Hashim F, et al. Clinical feasibility of synthetic MRI in multiple sclerosis: a diagnostic and volumetric validation study. *Am J Neuroradiol* 2016;37:1023–1029.
15. Birkel C, Langkammer C, Golob-Schwarzl N, et al. Effects of formalin fixation and temperature on MR relaxation times in the human brain: formalin fixation MR relaxation mechanisms. *NMR Biomed* 2016;29: 458–465.
16. Tustison NJ, Cook PA, Klein A, et al. Large-scale evaluation of ANTs and FreeSurfer cortical thickness measurements. *Neuroimage* 2014; 99:166–179.
17. Polman CH, Reingold SC, Banwell B, et al. Diagnostic criteria for multiple sclerosis: 2010 revisions to the McDonald criteria. *Ann Neurol* 2011;69:292–302.
18. Lublin FD, Reingold SC, Cohen JA, et al. Defining the clinical course of multiple sclerosis: the 2013 revisions. *Neurology* 2014;83:278–286.
19. Kurtzke JF. Rating neurologic impairment in multiple sclerosis: an expanded disability status scale (EDSS). *Neurology* 1983;33: 1444–1452.
20. Langdon D, Amato M, Boringa J, et al. Recommendations for a Brief International Cognitive Assessment for Multiple Sclerosis (BICAMS). *Mult Scler J* 2012;18:891–898.
21. Lezak MD, Howieson DB, Bigler ED, Tranel D. *Neuropsychological assessment*. New York, NY: Oxford University Press, 2012.
22. Ambarki K, Lindqvist T, Wåhlin A, et al. Evaluation of automatic measurement of the intracranial volume based on quantitative MR imaging. *Am J Neuroradiol* 2012;33:1951–1956.
23. Ashburner J, Friston KJ. Unified segmentation. *Neuroimage* 2005;26 (3):839–851.
24. Schmidt P, Gaser C, Arsic M, et al. An automated tool for detection of FLAIR-hyperintense white-matter lesions in multiple sclerosis. *Neuroimage* 2012;59:3774–3783.
25. Jenkinson M, Beckmann CF, Behrens TEJ, et al. FSL. *Neuroimage* 2012;62:782–790.
26. Yushkevich PA, Piven J, Hazlett HC, et al. User-guided 3D active contour segmentation of anatomical structures: significantly improved efficiency and reliability. *Neuroimage* 2006;31:1116–1128.
27. Benjamini Y, Hochberg Y. Controlling the false discovery rate: a practical and powerful approach to multiple testing. *J R Stat Soc Series B Stat Methodol* 1995;57:289–300.
28. Laule C, Leung E, Li DK, et al. Myelin water imaging in multiple sclerosis: quantitative correlations with histopathology. *Mult Scler J* 2006;12:747–753.
29. Schmierer K, Scaravilli F, Altmann DR, et al. Magnetization transfer ratio and myelin in postmortem multiple sclerosis brain. *Ann Neurol* 2004;56:407–415.
30. Schmierer K, Tozer DJ, Scaravilli F, et al. Quantitative magnetization transfer imaging in postmortem multiple sclerosis brain. *J Magn Reson Imaging* 2007;26:41–51.
31. Glasser MF, Van Essen DC. Mapping human cortical areas in vivo based on myelin content as revealed by T1- and T2-weighted MRI. *J Neurosci* 2011;31:11597–11616.
32. Righart R, Biberacher V, Jonkman LE, et al. Cortical pathology in multiple sclerosis detected by the T1/T2-weighted ratio from routine magnetic resonance imaging: cortical pathology in MS. *Ann Neurol* 2017;82:519–529.
33. Hagiwara A, Hori M, Cohen-Adad J, et al. Linearity, bias, intrascanner repeatability, and interscanner reproducibility of quantitative multidynamic multiecho sequence for rapid simultaneous relaxometry at 3 T: a validation study with a standardized phantom and healthy controls. *Invest Radiol* 2019;54:39–47.
34. Vavasour IM, Clark CM, Li DKB, MacKay AL. Reproducibility and reliability of MR measurements in white matter: clinical implications. *Neuroimage* 2006;32:637–642.
35. Levesque IR, Chia CLL, Pike GB. Reproducibility of in vivo magnetic resonance imaging-based measurement of myelin water. *J Magn Reson Imaging* 2010;32:60–68.
36. Nguyen TD, Deh K, Monohan E, et al. Feasibility and reproducibility of whole brain myelin water mapping in 4 minutes using fast acquisition with spiral trajectory and adiabatic T2prep (FAST-T2) at 3T. *Magn Reson Med* 2016;76:456–465.
37. Deoni SCL, Williams SCR, Jezzard P, et al. Standardized structural magnetic resonance imaging in multicentre studies using quantitative T1 and T2 imaging at 1.5 T. *Neuroimage* 2008;40:662–671.
38. Kolind S, Matthews L, Johansen-Berg H, et al. Myelin water imaging reflects clinical variability in multiple sclerosis. *Neuroimage* 2012;60 (1):263–270.
39. Deoni SCL, Matthews L, Kolind SH. One component? Two components? Three? The effect of including a non-exchanging “free” water component in multicomponent driven equilibrium single pulse observation of T1 and T2. *Magn Reson Med* 2013;70:147–154.
40. Benedict RB, Weinstock-Guttman B, Fishman I, et al. Prediction of neuropsychological impairment in multiple sclerosis: comparison of conventional magnetic resonance imaging measures of atrophy and lesion burden. *Arch Neurol* 2004;61:226–230.
41. Ouellette R, Bergendal Å, Shams S, et al. Lesion accumulation is predictive of long-term cognitive decline in multiple sclerosis. *Mult Scler Relat Disord* 2018;21:110–116.
42. Laule C, Vavasour IM, Moore GRW, et al. Water content and myelin water fraction in multiple sclerosis. *J Neurol* 2004;251:284–293.

43. Vavasour IM, Tam R, Li DK, et al. A 24-month advanced magnetic resonance imaging study of multiple sclerosis patients treated with alemtuzumab. *Mult Scler* 2019;25:811–818.
44. Kolind S, Matthews L, Johansen-Berg H, et al. Myelin water imaging reflects clinical variability in multiple sclerosis. *Neuroimage* 2012;60:263–270.
45. Kolind S, Seddigh A, Combes A, et al. Brain and cord myelin water imaging: a progressive multiple sclerosis biomarker. *Neuroimage Clin* 2015;9:574–580.
46. Barker GJ, Tofts PS, Gass A. An interleaved sequence for accurate and reproducible clinical measurement of magnetization transfer ratio. *Magn Reson Imaging* 1996;14:403–411.
47. Hayton T, Furby J, Smith KJ, et al. Grey matter magnetization transfer ratio independently correlates with neurological deficit in secondary progressive multiple sclerosis. *J Neurol* 2009;256:427–435.
48. Girard OM, Prevost VH, Varma G, et al. Magnetization transfer from inhomogeneously broadened lines (ihMT): experimental optimization of saturation parameters for human brain imaging at 1.5 Tesla: optimizing saturation parameters for ihMT brain imaging at 1.5T. *Magn Reson Med* 2015;73:2111–2121.
49. Van Obberghen E, Mchinda S, le Troter A, et al. Evaluation of the sensitivity of inhomogeneous magnetization transfer (ihMT) MRI for multiple sclerosis. *Am J Neuroradiol* 2018;39:634–641.
50. Granberg T, Fan Q, Treaba CA, et al. In vivo characterization of cortical and white matter neuroaxonal pathology in early multiple sclerosis. *Brain* 2017;140:2912–2926.
51. Arshad M, Stanley JA, Raz N. Test-retest reliability and concurrent validity of in vivo myelin content indices: myelin water fraction and calibrated $T_1 w/T_2 w$ image ratio. *Hum Brain Mapp* 2017;38:1780–1790.
52. MacKay AL, Laule C. Magnetic resonance of myelin water: an in vivo marker for myelin. *Brain Plast* 2016;2:71–91.